Distributed Primary and Secondary Power Sharing in a Droop-Controlled LVDC Microgrid with Merged AC and DC Characteristics

Peyghami, Saeed; Mokhtari, Hossein; Loh, Poh Chiang; Davari, Pooya; Blaabjerg, Frede

Published in:
IEEE Transactions on Smart Grid

DOI (link to publication from Publisher):
10.1109/TSG.2016.2609853

Publication date:
2018

Document Version
Accepted author manuscript, peer reviewed version

Distributed Primary and Secondary Power Sharing in a Droop-Controlled LVDC Microgrid with Merged AC and DC Characteristics

Saeed Peyghami-Akhuleh[1], *Student Member, IEEE,* Hossein Mokhtari[1], *Senior Member, IEEE,* Poh Chiang Loh[2], Pooya Davari[2], *Member, IEEE,* and Frede Blaabjerg[2], *Fellow, IEEE*[1]

***Abstract*— In an ac microgrid, a common frequency exists for coordinating active power sharing among droop-controlled sources. A common frequency is absent in a dc microgrid, leaving only the dc source voltages for coordinating active power sharing. That causes sharing error and poorer voltage regulation in dc microgrids, which in most cases, are solved by a secondary control layer reinforced by an extensive communication network. To avoid such an infrastructure and its accompanied complications, this paper proposes an alternative droop scheme for low-voltage dc (LVDC) microgrid with both primary power sharing and secondary voltage regulation merged. The main idea is to introduce a non-zero unifying frequency and a second power term to each dc source by modulating its converter with both a dc and a small ac signal. Two droop expressions can then be written for the proposed scheme, instead of the single expression found in the conventional droop scheme. The first expression is for regulating the ac frequency and active power generated, while the second is for relating the dc voltage to the second power term. The outcomes are better active power sharing and average voltage regulation in the dc microgrid, coordinated by the common injected ac frequency. These expectations have been validated by results obtained from simulations.**

***Index Terms*— distributed secondary control, LVDC microgrid, line impedance effects, droop control.**

I. Introduction

The concept of microgrids has been introduced for improving reliability, power quality, efficiency, and environmental friendliness [1]–[5]. Most studies have however focused on ac microgrids, but may gradually deviate to dc microgrids as power conversion technology advances. Some present dc applications include data centers [6], space explorations [7], offshore wind farms [8], electrical supplies on ships [9], electric vehicles [10], and HVDC transmission systems [11], with the scope of application likely to expand as most renewable sources, electronic loads and converter-linked electrical machines have a natural dc coupling [12]. Energy saving can therefore be realized, if these sources and loads are connected to the dc grids, even though dc-dc converters may still be needed [13].

DC microgrids will however still require proper power management, which like in ac microgrids, is usually achieved by three levels of hierarchical control, named respectively as the tertiary, secondary and primary layers. The first two upper layers usually require communication links [14]–[17], while the lower primary layer is usually distributed with no communication links. The primary layer is also responsible for proper power sharing, which in most cases, is maintained proportional to the ratings of the sources. Such proportional sharing can conveniently be ensured by droop control with virtual output impedances usually inserted to the sources [18]–[23]. The tradeoff is slight voltage droops at the sources, which if not acceptable, can be restored by the secondary layer through coordination using communication links [18], [24]–[27].

No doubt, these methods are simple and well developed, but they still introduce some inaccuracies to the power sharing and voltage regulation. These inaccuracies are mostly related to the non-negligible and variable line impedances [24]–[27], which in practice, will cause output voltage mismatches among the sources, even if they deliver the same power to the same Point of Common Coupling (PCC). Possible solutions for the above problems have been reviewed in [16] with some centralized schemes found to rely on an extensive communication network and other decentralized schemes found to base on the droop principle [28]–[31]. For example, a centralized secondary control has been recommended in [32], where voltages within the microgrid have been measured for computing a restoration term to be sent to all sources. Adaptive droop control in [33] has also been proposed for improving the microgrid performance, but has unfortunately neglected the line impedances. High droop gains are then suggested in [16] for mitigating power sharing inaccuracy caused by the line impedances.

A "mixed" scheme has also been proposed in [34], where a communication network is still needed within the microgrid, but the centralized secondary functionality has somehow been embedded in the converter of each source. Its reliance on point-to-point communication has however still subject it to link failures, which when happened, will bring down the entire microgrid. The same problem is faced by [35] because of its reliance on extensive communication, even though it has taken the effects of line impedances into account for improved accuracy. Voltage regulation wise, [35] and [36] have relied

[1] [1]Saeed Peyghami-Akhuleh and Hossein Mokhtari are with the Department of Electrical Engineering, Sharif University of Technology, Iran (e-mail: saeed_peyghami@ee.sharif.edu, mokhtari@sharif.edu).

[2]Poh Chiang Loh, Pooya Davari, and Frede Blaabjerg are with the Institute of Energy Technology, Aalborg University, Denmark (e-mail: pcl@et.aau.dk, pda@et.aau.dk, fbl@et.aau.dk).

on the same redefined requirement of regulating the average voltage of the whole microgrid at a certain global set-point value, which again requires communication links.

Although less common, independence of communication is possible, as demonstrated in [37], where a current-sharing technique based on frequency encoding of sharing information has been introduced. Another technique, named as power talk, has also been mentioned in [38], where sources in the dc microgrid "talk" to each other by modulating their respective power levels without demanding for external communication links. The technique is however prone to load or other grid parameter changes, which in practice, are unpredictable. The frequency-based power sharing technique proposed in [20] and [39], and later reapplied to LVDC microgrids in [40], may therefore be more appealing, since it is based on the same conventional droop principle, while yet ensuring very low affection towards variations. Some problems with the technique however exist, as explained below.

a) The technique in [20], [39], [40] is developed with inductive connecting lines assumed. Simulation is however performed with pure resistive lines. The results obtained therefore do not prove the technique adequately, since different line natures will give rise to different droop expressions. For the LVDC microgrids considered, both theory and simulation must be developed with resistive lines.
b) Power angle between any two converters (δ) depends on the dc demand of the microgrids. It cannot be more than 90°, because of the usual steady-state stability limit [41]. Relationship between this angle and magnitude of the injected voltage should therefore be further elaborated.
c) Voltage droop coefficients should be selected proportional to the power ratings of the converters. This selection is however presently not clear, and should hence be further explained.
d) The present belief is high-frequency droop gain causes angular instability. However, as explained later, angular instability is directly related to the magnitude of the injected voltage and the voltage droop gain.

To address the above issues, a new power sharing control with merged ac and dc characteristics has been proposed for LVDC microgrids. The proposed method uses two conventional droop controllers for performing duties of both primary and secondary layers in a distributed manner. It can therefore achieve the following advantages simultaneously:

- Accurate proportional power sharing among the distributed generators (DGs) or sources.
- Proper regulation of the average dc bus voltage.
- Reliability improvement even without communication links.

These advantages are illustrated systematically, after briefly describing the dc power flow theory in Section II. Section III then explains proposed power management system with possible options for inserting ac characteristics to the (otherwise pure) LVDC microgrids. This is followed by an extensive discussion of the distributed primary and secondary droop controllers in Section IV and small signal stability of the proposed control system in Section V, before results for validating them are described in Section VI. Last but not least, Section VII concludes the findings contributed by the investigation.

II. DC Power Flow Theory

A block diagram of a typical dc system with distributed loads is shown in Fig. 1. In this system, DGs are connected to the local loads as well as a remote load through the feeders at PCC. From the electric circuit theory for dc power flow analysis, the dc current of i^{th} feeder (i.e., I_{fi}) can be determined as:

$$I_{fi} = \frac{V_i - V_{PCC}}{r_i}, \quad i = 1, 2, ..., N \tag{1}$$

where V_i is the dc voltage of the i^{th} converter, V_{PCC} is the dc voltage of the PCC, and r_i as the resistance of the i^{th} feeder. According to (1), if all converters regulate their output voltage at the same reference value, the current of each feeder will be inversely proportional to its resistance. Considering local loads at the output terminal of the converters, the output dc current of the i^{th} converter I_i can be calculated as:

$$I_i = I_{fi} + I_{li}, \quad i = 1, 2, ..., N \tag{2}$$

where I_{li} is the i^{th} local load current.
Substituting (1) into (2), the output current of the i^{th} converter can be determined as:

$$I_i = \frac{V_i - V_{PCC}}{r_i} + I_{li}, \quad i = 1, 2, ..., N \tag{3}$$

Therefore, the output current of the converters is related to the dc voltage, feeder resistance, and local load current. In practice, the output current of the DGs is limited to the rated value. To prevent overstressing the converters, a current (power) sharing technique is required to control the power flow in the grid. The power sharing system controls the power flow by adjusting the dc voltages at desirable values to have a suitable current sharing. However, the voltages have to remain within acceptable limits. DC voltage based droop methods have been carried out to control the power sharing in dc grids [18]–[23]. These methods are analogous with the conventional frequency droop in synchronous generators. However, unlike the frequency in ac grids, dc voltage is a local variable, hence, the performance of the droop methods based on the dc voltage in dc grids are not satisfactory. The major disadvantages of this method are poor current sharing and large voltage drops in the grid [35], [42]–[44]. To improve the effectiveness of this technique, complementary control loops based on communicating among converters are introduced in literature [16]. However, the communication link affects the reliability of the system.

Finally, power sharing in dc grids suffers from the lack of a global variable to synchronize the DGs. In this paper, instead of the dc voltage, a new virtual frequency is employed to control the power sharing in dc grids. The virtual frequency droop is analogues to the frequency droop method in ac power

systems. The main advantages of the proposed approach are accurate current sharing and small voltage drop in the terminals as well as regulated average voltage in the grid.

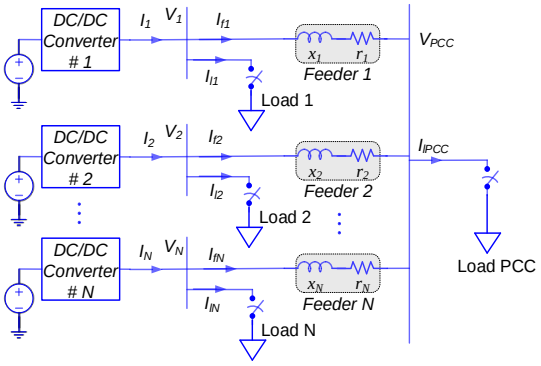

Fig. 1. Block diagram of a dc microgrid with distributed loads.

III. Proposed Power Management System

For simplicity, a dc microgrid with two DG like the one in Fig. 2 is considered to show the effectiveness of the control system. As described in dc power flow section, the dc currents generated by two converters are inversely proportional to the line resistance. Therefore, the output currents of the converters must be controlled by maintaining their output voltage. The proposed control system for power sharing among DGs and also voltage regulation in the system is represented in Fig. 3. The main idea is to add a small ac voltage to the dc voltage reference and adjusting the dc voltage reference by a suitable ac variable (i.e, *X* in Fig. 3). This variable needs to contain the line resistance information. The possible options to adjust the dc voltage reference are: (a) frequency of injected voltage (*f*) that is related to the output dc current of converter, (b) angle of injected voltage (δ), and (c) injected ac voltage ($\tilde{v}$).

Option (a) is not suitable for adjusting the dc voltage, since the frequency has the same value all over the grid. Also the angle of voltage (i.e., option (b)) is a time variant variable and cannot fix the output voltage of converters. However, option (c) sounds to be a promising option to control the voltage of DGs. The injected ac voltage makes a small ac current flow in the microgrid.

Applying the control system for both converters, the output voltage contains both dc and ac components. Fig. 4 illustrates the ac equivalent circuit of the grid shown in Fig. 2. The output instantaneous ac current of each unit and also the ratio of these currents can be obtained as:

$$\tilde{i}_k = \frac{|\tilde{v}_k - \tilde{v}_{PCC}|}{|r_k + jx_k|}, \quad k = 1,2 \tag{4}$$

$$\frac{\tilde{i}_1}{\tilde{i}_2} = \frac{|\tilde{v}_1 - \tilde{v}_{PCC}||r_2 + jx_2|}{|\tilde{v}_2 - \tilde{v}_{PCC}||r_1 + jx_1|} \tag{5}$$

where r_k and x_k are the resistance and reactance of k^{th} line, respectively and $\tilde{v}$ and $\tilde{i}$ are the instantaneous ac voltage and current in the microgrid.

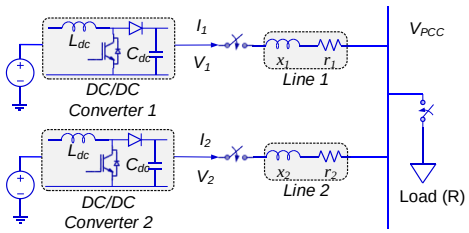

Fig. 2. Block diagram of a simplified dc microgrid for two converters.

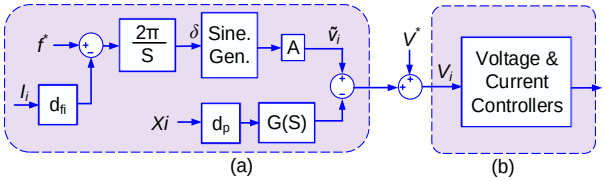

Fig. 3. Control structure for i^{th} converter (a) sharing control (secondary and primary) and inner control loops, and (b) inner voltage and current loops.

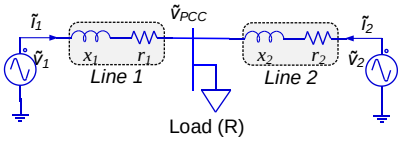

Fig. 4. AC equivalent circuit of the simplified dc microgrid shown in Fig. 2.

The magnitude of the injected ac voltages will be selected with the same value for both converters. Therefore, based on (5) the ratio of the ac currents is inversely proportional to the line impedances as,

$$\frac{\tilde{i}_1}{\tilde{i}_2} = \frac{\sqrt{r_2^2 + x_2^2}}{\sqrt{r_1^2 + x_1^2}} \tag{6}$$

On the other hand, in low voltage (LV) systems, with frequency equal to 50 Hz, the *X*/*R* ratio of lines is small (e.g., 0.083/0.65 = 0.12) [15], therefore, (6) can be rewritten as,

$$\frac{\tilde{i}_1}{\tilde{i}_2} = \frac{r_2}{r_1} \tag{7}$$

Since the ac currents contain the information of the line resistance, the injected active and reactive power might be sufficient variables to adjust the dc voltages. As already mentioned, the use of active power has been introduced before [40], however active power in low voltage (LV) systems especially with low injected frequency (i.e., 20 Hz in [40]) is not proportional to the frequency [15], [19]. In spite of using virtual reactance to decouple the active and reactive power in LVAC systems [15], virtual reactance cannot satisfy the proposed merged droop method. Because based on (6), using virtual reactance with dominant value debilitates the effect of resistance and the ratio of ac currents would be proportional to the virtual reactance. Therefore, injected active power cannot adjust the dc voltage in the merged droop method. On the other hand, in the LV microgrids, the reactive power is proportional to the frequency [15], [19], [45]. Hence, in this paper, the reactive power dispatched between converters by frequency- current droop is used to control the dc power

sharing. The details of the proposed control system are described in the next section.

IV. Merged AC/DC Primary and Secondary Droop Controllers

The proposed approach is based on coordinating the power sharing among the DGs applying the conventional ac power sharing approach in the dc microgrid with the frequency of a small injected voltage at the voltage controlled buses.

A. Power sharing control

By injecting a small ac voltage at the voltage controlled buses, and controlling the small ac power between the converters, the frequency-based droop control scheme can properly control the dc power. Fig. 3 shows the adopted control scheme. The power control system in Fig. 3 (a) manages the current with two conventional droop control schemes as a merged ac/dc droop method: (1) frequency-current droop control, and (2) voltage -power droop control.

1) Frequency- current droop control (d_f)

This control method determines the frequency and the angle of the injected ac voltage based on the output dc current of the converter. Based on droop characteristics as depicted in Fig. 5 both converters must have a proportional current at the steady state condition. Frequency droop gains can be defined as (8).

$$d_{fi} = \frac{f_{\max} - f_{\min}}{I_{ni}}; \quad i = 1, 2, ..., N \tag{8}$$

where f_{max}/f_{min} are the maximum/minimum frequency for tuning the droop gain and I_{ni} is the rated current of i^{th} converter.

Let f^* be the nominal frequency of the injected signal and $d_{f1} = d_{f2} = d_f$. If the output currents of converter 1 and 2 are I_1 and I_2 respectively, then

$$f_1 = f^* - d_f I_1 \tag{9}$$

$$f_2 = f^* - d_f I_2 \tag{10}$$

if $I_1 > I_2$ then $f_1 > f_2$ and $\Delta f = f_1 - f_2$. The difference in the frequency manifests itself as a phase difference between the two injected voltage signals as:

$$\delta = 2\pi \int \Delta f dt \tag{11}$$

$$\delta = d_f (I_1 - I_2) t \tag{12}$$

This difference in the voltage angle causes a small power flow between the units. By setting the dc voltage reference based on this small power, proper power sharing is obtained.

2) Voltage- power droop control (d_p)

As depicted in Fig. 6, the slope of the output characteristics of each converter has to automatically change in order to have a proportional output current between the converters. The output voltage of i^{th} converter (V_i) can be calculated as:

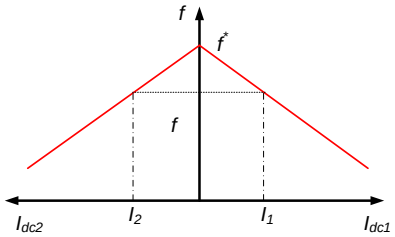

Fig. 5. Frequency- current droop characteristics used in dc microgrid.

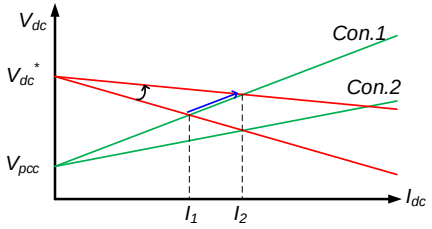

Fig. 6. Voltage- current droop characteristics; red lines are output droop characteristics of converters, and green lines illustrate (13).

$$\begin{aligned} V_i &= V_{PCC} + r_i I_i; \quad i = 1, 2 \\ V_{PCC} &= R(I_1 + I_2) \end{aligned} \tag{13}$$

From the voltage droop control loop in Fig. 3 (a), considering unity gain for the inner voltage and current loops and also for $G(s)$ at the steady state, the output voltage of i^{th} converter can be found as:

$$V_i = V^* - d_p X_i; \quad X_i = Q_i \tag{14}$$

where V^* is the rated dc voltage and Q_i is the injected reactive power by the i^{th} converter. Q_i can be calculated as:

$$Q_i = \frac{|\tilde{v}_i| . |\tilde{v}_j|}{2r} \sin(\angle\tilde{v}_i - \angle\tilde{v}_j) \tag{15}$$

where $|x|$ and $\angle x$ denote the magnitude and phase of x, indexes of i and j indicate the sending end and receiving end of line, and r is the line resistance between two buses.

Equation (14) can be rearranged based on the output current like (16) in order to achieve the adjustable droop gain d_{pi} as (17).

$$V_i = V^* - \left(\frac{d_p Q_i}{I_i} \right) I_i \tag{16}$$

$$V_i = V^* - d_{pi} I_i \tag{17}$$

B. Voltage regulation

In the prior-art method for voltage regulation in dc microgrids it is mandatory to control the average voltage of voltage controlled buses at the reference value [16], [32], [35]. In both centralized and decentralized schemes for voltage regulation, some communications between units are required to measure the voltages and regulate the average value which extremely affects the reliability and might cause the failure of the corresponding unit, overstressing other units, and potentially leading to instability. However, in the proposed

control strategy, the average voltage (V_{avg}) of the voltage controlled buses is:

$$V_{avg} = \frac{1}{n}\sum_{i=1}^{n} V_i = \frac{1}{n}\sum_{i=1}^{n}(V^* - d_p Q_i) = V^* - \frac{d_p}{n}\sum_{i=1}^{n} Q_i \qquad (18)$$

The reactive power consumption of the lines is negligible since the *X*/*R* ratio of the lines and the injected ac voltage are small. Furthermore, the dc loads in dc microgrids including resistive loads and Constant Power Loads (CPLs) consume/-generate zero and small reactive power respectively. Moreover, in dc microgrids, the dc link voltage is regulated by the source converters as Line Regulating Converters (LRCs). The dc link capacitor of the CPLs can have a small value in DC systems [46], [47], and hence, the reactive power of the loads cannot extensively affect the average voltage of the microgrid. Therefore, unlike conventional droop method, as stated in (19), the proposed droop approach can regulate the average voltage near the reference value without supplementary controllers.

C. Selecting injected frequency and voltage

The injected frequency directly affects the decoupling between active and reactive power in the lines, and tracking performance of the inner voltage compensator. The inner voltage and control loops are explained in Appendix. Therefore, to comply with these factors, this value should be selected as small as possible. In this paper, like an ac microgrid, f = 50 Hz is considered as the frequency of the injected ac voltage.

Notably, due to the stability issues, the amplitude of the injected voltage (i.e., A in Fig. 3(a)) is more important than the injected frequency. The main restrictions on (A) are the maximum allowable ripple on dc bus, the maximum transmission capability of the line, transient stability of virtual ac system, and dynamic stability of power management system. Since there is no recommended standard for power quality of dc distribution systems in determining the maximum ripple of the dc voltage, it should be as small as possible. However, it shouldn't be very small either, since its detection will be noise sensitive.

The maximum transmission capability of the reactive power is limited by the static stability limit of the line which is defined as the maximum of the injected reactive power in (15) [41]. Here, the magnitude of $\tilde{v}_i$ and $\tilde{v}_j$ is equal to A. According to Fig. 2, the resistance between two converter is ($r = r_1 + r_2$). The maximum of the reactive power Q_m is occurred at $\delta = 90^o$ and can be calculated as:

$$Q_m = \frac{|\tilde{v}_i|.|\tilde{v}_j|}{2r} sin\,\delta\,|_{\delta=90^o} = \frac{A^2}{2(r_1 + r_2)} \qquad (19)$$

On the other hand, the maximum required reactive power Q_{max} at $R = R_{min}$ can be calculated by (13) and (14) as (20), where $k = \frac{I_{n1}}{I_{n2}} = \frac{d_{f2}}{d_{f1}}$.

$$Q_{\max} = \frac{V^*}{d_p}\frac{r_2 - r_1 k}{2R_{\min}(1+k) + r_1 k + r_2} \qquad (20)$$

Because of the static stability, Q_{max} must be equal to Q_m. Furthermore, to have the angular stability in the ac system it should be less than Q_m. Practically, Q_{max} designed to be about the 60% of the Q_m [41]. Furthermore, the small reactive power of loads Q_l can limit the maximum transmission capability of the reactive power. Therefore, the amplitude of the injected voltage (A) and the voltage droop gain (d_p) must meet the following condition:

$$A^2 \geq \frac{2(r_1 + r_2)}{0.6}\left(\frac{2V^*}{d_p}\frac{(r_2 - r_1 k)}{2R_{\min}(1+k) + r_1 k + r_2} + Q_l\right) \qquad (21)$$

D. Synchronizing the ac voltages

Like ac microgrids, the injected ac voltage by the converters has to be synchronized with the ac component of the grid voltage at the startup time. The phase of the connection bus voltage can be extracted using a Phase Locked Loop (PLL) block to synchronize the injected ac signal with the grid. After synchronizing, all units operate based on their droop characteristics to support the load like a grid supporting voltage source converter in ac microgrids [15].

V. Small Signal Stability and Controller Design

For simplicity, a dc microgrid with two DGs like the one presented in Fig. 2 (a), is considered, and modeled for stability studies and control system design. From Fig. 3, the power angles of each unit (δ_1, δ_2) are:

$$\begin{aligned} \delta_1 &= \frac{2\pi}{s}\left(f^* - d_{f1} I_1\right) \\ \delta_2 &= \frac{2\pi}{s}\left(f^* - d_{f2} I_2\right) \end{aligned} \qquad (22)$$

Therefore the power angle between two DGs and the small variation of it are described as:

$$\delta = \delta_1 - \delta_2 = \frac{2\pi}{s}\left(d_{f2} I_2 - d_{f1} I_1\right) \qquad (23)$$

$$\Delta\delta = \frac{2\pi}{s}\left(d_{f2}\Delta I_2 - d_{f1}\Delta I_1\right) \qquad (24)$$

where $\Delta(.)$ depicts the small variation of each variables. From the ac power flow analysis, the ac power generated by DGs, Q_1 and Q_2 are:

$$\begin{aligned} Q_1 &= -\frac{A^2/2}{r_1 + r_2}\sin\delta \\ Q_2 &= \frac{A^2/2}{r_1 + r_2}\sin\delta \end{aligned} \qquad (25)$$

where A is the magnitude of ac voltage. The effect of line inductances is negligible. The linear form of (25) is shown in (26) and k_δ at the power angle of δ_o can be calculated as (27).

$$\begin{cases} \Delta Q_1 = -k_\delta \Delta\delta \\ \Delta Q_2 = +k_\delta \Delta\delta \end{cases} \qquad (26)$$

$$k_\delta = \frac{A^2}{2(r_1+r_2)}\cos\delta_0 \tag{27}$$

The inner voltage loop control references calculated by the power sharing control system for both converters are:

$$\begin{cases} V_1 = V^* - d_p Q_1 G(s) \\ V_2 = V^* - d_p Q_2 G(s) \end{cases} \tag{28}$$

where $G(s)$ is a low pass filter to eliminate the high frequency component of Q ($G(s) = \frac{\omega_c}{S+\omega_c}$). The linear form of (28) is:

$$\begin{cases} \Delta V_1 = -d_p \Delta Q_1 G(s) \\ \Delta V_2 = -d_p \Delta Q_2 G(s) \end{cases} \tag{29}$$

Therefore, the linear form of equations of (13) is:

$$\begin{cases} \Delta V_1 = (r_1+R_0)\Delta I_1 + R_0\Delta I_2 + (I_{10}+I_{20})\Delta R \\ \Delta V_2 = R_0\Delta I_1 + (r_2+R_0)\Delta I_2 + (I_{10}+I_{20})\Delta R \end{cases} \tag{30}$$

where I_{10} and I_{20} are the dc current of each converter at R_0. Combining equations (24), (26), (29) and (30) and taking into considering $\Delta\delta$ as a state variables and ΔR as a disturbance, the state space representation can be obtained as (31).

$$\frac{d^2\Delta\delta}{dt^2} + \omega_c\frac{d\Delta\delta}{dt} + \frac{\beta}{\alpha}\Delta\delta = -\frac{\gamma\omega_c}{\alpha}\Delta R - \frac{\gamma}{\alpha}\frac{d\Delta R}{dt} \tag{31}$$

The characteristic equation for closed loop system in Laplace domain is (s is Laplace operator):

$$S^2 + \omega_c S + \frac{\beta}{\alpha} = 0 \tag{32}$$

$$\alpha = r_1 r_2 + (r_1+r_2)R_0 \tag{33}$$

$$\beta = 2\pi\omega_c k_\delta d_{f1} d_p (2R_0(k+1) + r_1 k + r_2) \tag{34}$$

$$\gamma = 2\pi(r_1+r_2)(I_{10}+I_{20}) \tag{35}$$

According to (20), (25) and (27) k_δ can be determined as:

$$k_\delta = \frac{1}{d_p}\sqrt{\left(\frac{A^2 d_p}{2(r_1+r_2)}\right)^2 - (\Delta V_{max})^2} \tag{36}$$

Therefore, the control parameters of the power sharing system are ω_c, A and d_p. According to (34) and (36), A^2 and d_p have the same effect on the dynamic behavior of the control system. Let consider a simple system with the parameters given in Table I. The dominant poles of the closed loop transfer function of the system can be determined by (32). The roots of this equation for different A^2d_p and ω_c are represented in Fig. 7. As it can be seen in Fig. 7, increasing ω_c moves the closed loop poles away from the origin to the left side of the S-plane. Therefore, the damping of the system is increased by increasing the ω_c. The effect of A^2d_p on the location of the poles is also demonstrated in Fig. 7. Increasing this term has reverse effect on both poles. For small A^2d_p, one of the poles is near the origin and it affects the damping of the system. Therefore, increasing this term moves the dominant pole away from the origin to increase the performance of the control system. As shown in Fig. 8 (a), the closed loop poles are not effectively affected by changing the load resistance. Therefore, the performance of the control system at different loading condition is guaranteed.

TABLE I
Specifications of DC Microgrid and Proposed Control System

Definition	Symbol	Value		
		Case I	Case II	Case III
Impedance of line 1	$r_1(\Omega)/L_1(\mu H)$	2/0	2/600	2/600
Impedance of line 2	$r_2(\Omega)/L_2(\mu H)$	4/0	4/900	1/400
Rated current of DGs	I_{n1}/I_{n2} (A)	7/7	5/10	10/5
Injected frequency	f^* (Hz)	50	50	50
Frequency limits	f_{max},f_{min}	50,49	50,48.5	50,48.5
Frequency droop gain	d_{f1},d_{f2} (Hz/A)	0.15, 0.15	0.3, 0.15	0.15, 0.3
-	A^2d_p	350	280	280
Voltage droop gain	d_p (V/VAR)	3.5	2.8	2.8
Injected voltage amplitude	A(V)	10	10	10
DC link voltage	V_{dc} (V)	700	700	700
Cut off frequency	ω_c (rad/sec)	35	35	35

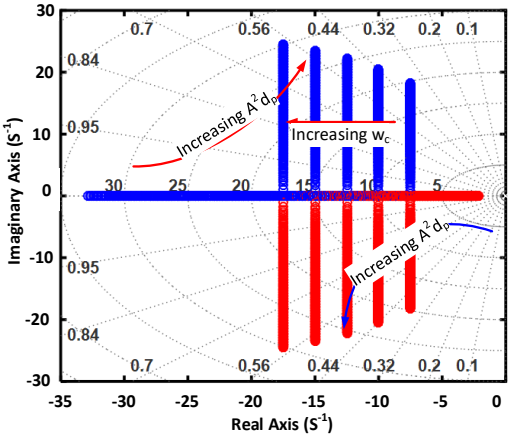

Fig. 7. Closed loop pole places, 80 <A^2d_p< 500, 20 < ω_c <4 0, R = 50 Ω.

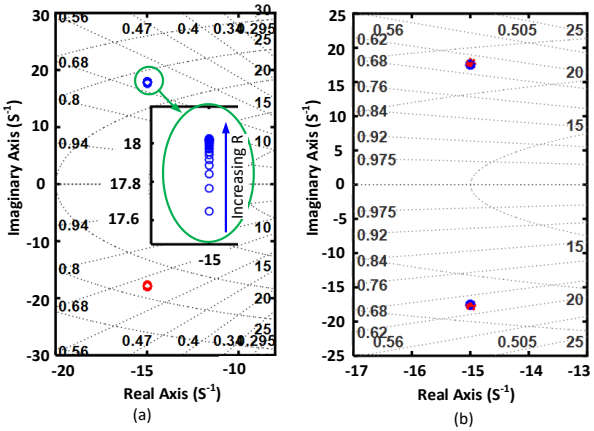

Fig. 8. Closed loop pole places; (a) effect of load resistance, A^2d_p =350, ω_c =35 rad/s, A=10 V, 50 < R < 500, (b) closed loop pole places for case I and II.

VI. Simulation Results

In order to demonstrate the performance of the proposed control approach at different working conditions, a simulation test system – like the one shown in Fig. 2 – with MATLAB-/Simulink is performed and three case studies are considered. In Case I, the performance of the proposed approach is compared with that obtained by the conventional droop method. Moreover, the applicability of the proposed method is illustrated in the presence of the resistive loads and CPLs considering the same capacity for the DGs and pure resistive lines. Case II is considered to show the performance of the proposed approach in the presence of the constant current loads as well as unequal DG capacity and low X/R ratio lines. Moreover, the viability of the proposed control system in the presence of renewable resources (e.g., PhotoVoltaic (PV)) is demonstrated in Case III. The parameters of the test system are given in Table I, and the specifications of the dc/dc converter of the DGs are given in the Appendix. Meanwhile, the pole placement approach is considered to design the control system. Closed loop poles in both cases are depicted in Fig. 8 (b). The cut off frequency (ϖ_c) is considered 35 rad/sec to eliminate the high frequency oscillations of the reactive power. A^2d_p is also determined to have a 0.7 of damping ratio in the power sharing control system. This value should satisfy the equation (21). There is no limit for the injected voltage amplitude (A), unless maximum allowable ripple on the dc voltage. In this study, A is considered to be 10 V (i.e., 1.4%).

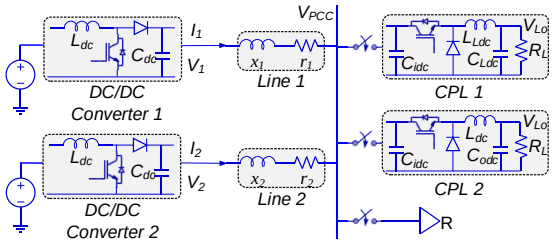

Fig. 9. Block diagram of a dc microgrid with resistive load and CPLs, R = 100 Ω, R_L = 125 Ω, L_{Ldc} = 100 µH, C_{Ldc} = 300 µF, C_{idc} = 100 µF , V_{Lo} = 500 V.

A. Case I:

In this case, a 100 Ω resistive load and 2×2 kW CPL are considered to show the performance of the control system in the presence of different loads and make a comparison with the conventional droop method. Fig. 9 shows the block diagram of the test system and the load specifications. Here, the first CPL is turned on at t = 1.5 sec and the second CPL is connected at t = 3 sec and disconnected at t = 4.5 sec.

As shown in Fig. 10, employing the conventional droop method causes unequal current sharing between the DGs as well as large voltage drops by increasing the load. As it can be seen in Fig. 10 (a), at 3 < t < 4.5 sec, the first DG supports more than 7 A and the other one support 5.5 A. Although the second DG can support more current, increasing the load causes overstressing the first DG. Therefore, the conventional droop method cannot sufficiently share the current/power between the DGs. Meanwhile, increasing the loads causes more voltage drop at the terminal voltages as it can be seen in Fig. 10 (b).

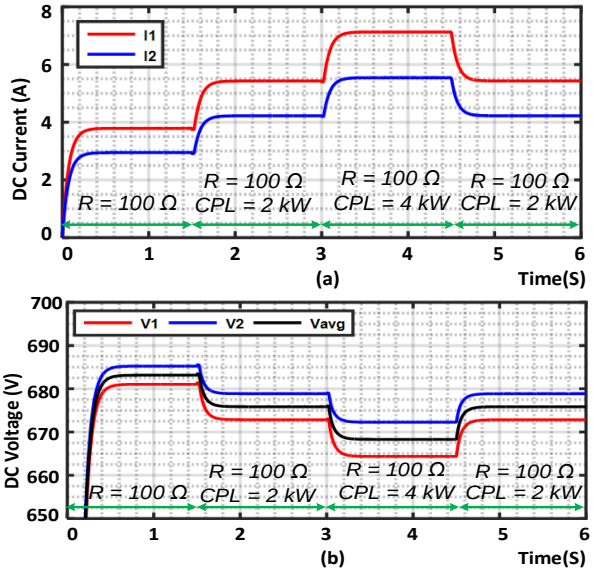

Fig. 10. Simulation results of Case I with Conventional Droop Method: (a) DC current, (b) DC voltage.

However, as shown in Fig. 11 (a) and (b), applying the proposed control method, current and power sharing are properly performed with both resistive loads and CPLs. Any load changes can be equally supported by both DGs at the steady state. Furthermore, the mean value of the dc voltages in Fig. 11 (c) shows small voltage variation at the terminal voltages and regulated average voltage at the reference value. The average voltage at heavy loading condition (i.e., 3 < t < 4.5 sec in Fig. 10 (a) and Fig. 11 (c)) is 668 V and 706 V in the conventional and the proposed droop method respectively which indicates the proper voltage regulation in the proposed method. The instantaneous voltages of DG1 and DG2 are shown in Fig. 11 (c). The frequencies of both voltages converge to the same stables value at steady state as shown in Fig. 11 (d). The frequency deviation from 50 Hz is relevant to the dc current of the loads. Since the frequency has the same value in the grid, the output current of the DGs can be equally dispatched by employing the frequency instead.

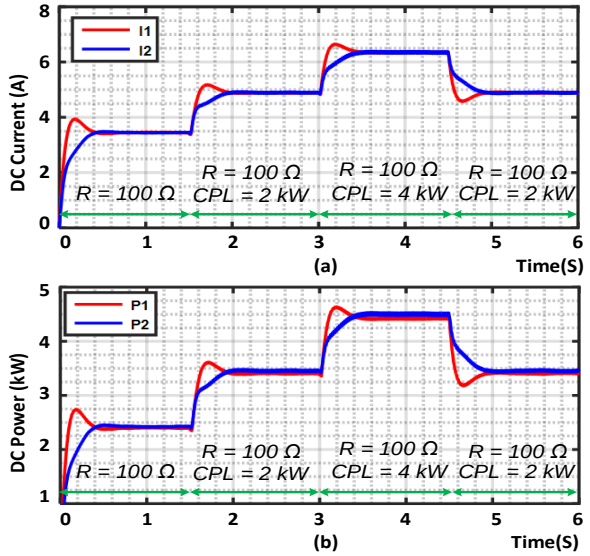

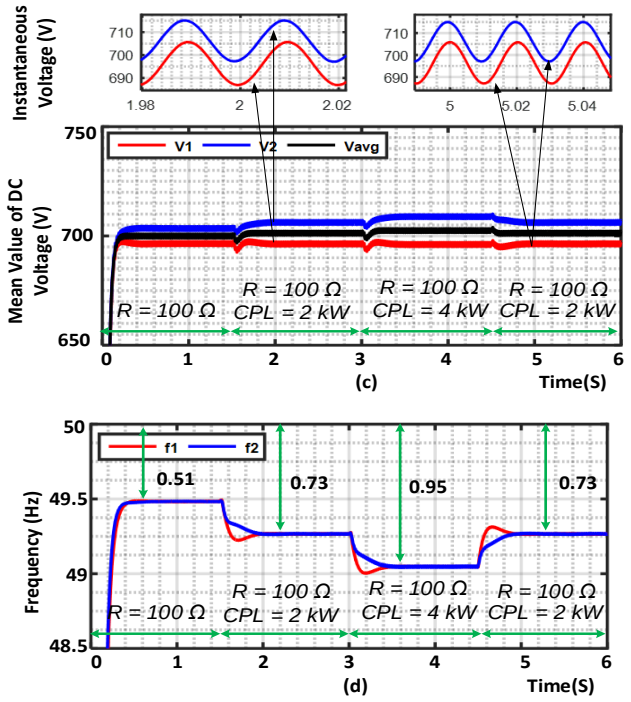

Fig. 11. Simulation results of Case I with Proposed Method: (a) DC current, (b) DC power, (c) mean values of DC voltage of DG1 and DG2 and average of these voltages (instantaneous values of the voltage of DG1 and DG2 are given at two time intervals), and (d) frequency of DG1 and DG2.

B. Case II:

In this case, the applicability of the proposed control system is demonstrated by considering unequal DG ratings and low X/R ratio line impedances in the presence of constant current load with a load profile as shown in Fig. 12. The system structure is similar to Case I, and the parameters are given in Table I. As shown in Fig. 13 (a) and (b), the sufficient current and power sharing between the DGs are obtained which are proportional to their ratings at different loading conditions. Fig. 13 (c) shows that the voltage profiles remain close to the reference value, and the average voltage is regulated at the reference value at different loading conditions. The instantaneous dc voltages of DG1 and DG2 are illustrated in Fig. 13 (c). Variations of the frequency in Fig. 13 (d) shows the demand of the system, where increasing the load causes a frequency drop. The reactive power of both DGs in Fig. 13 (e) shows that the summation of reactive powers is equal to zero, hence, the average of the voltages should remain at 700V. The power angle between the two DGs is shown in Fig. 13 (f).

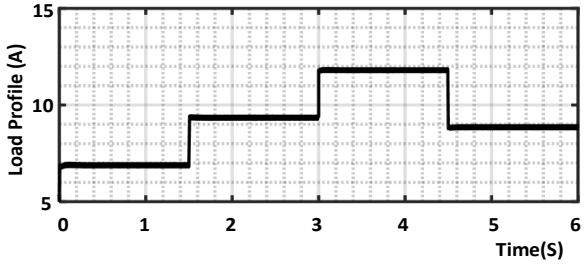

Fig. 12. Case II; Load current profile.

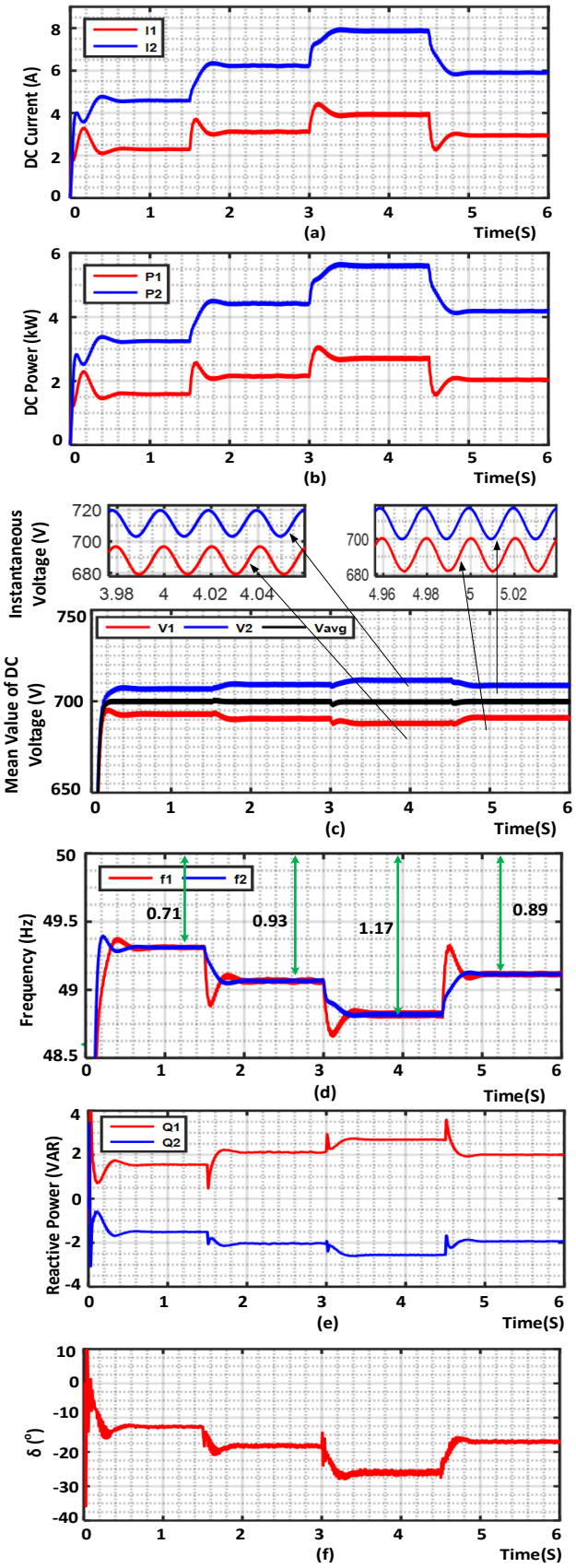

Fig. 13. Simulation results of Case II with proposed method; (a) DC current, (b) DC power, (c) mean values of DC voltage of DG1 and DG2 and average of these voltages (instantaneous values of the voltage of DG1 and DG2 are given at two time intervals), (d) Frequency, and (e) injected reactive power, and (f) Power angle between DG1-DG2.

C. Case III:

In this case, the viability of the proposed control strategy is further demonstrated in the presence of Photovoltaic (PV) array as a renewable energy resource. Renewable resources operating in Maximum Power Point Tracking (MPPT) mode are behaving as a grid feeding converter for injecting the MPPT power into the grid [15]. In this case a 4 kW buck based PV converter is connected to the dc microgrid shown in Fig. 9. Here, the capacity of the first converter is two times of the second one.

The simulation results are given in Fig. 14. In the beginning, a 4.9 kW load is supplied by the 2.6 kW PV and two converters. At t = 1.5 sec, the PV power is decreased by 1.1 kW. Moreover, a 2 kW CPL is connected at t = 3 sec, and the PV power is increased by 1.1 kW at t = 4.5 sec. The dc current and power of converters are shown in Fig. 15(a) and (b) implying proportional power and current sharing between the converters in the presence of the PV unit. As it can be seen in Fig. 14(a), by increasing/decreasing the PV power (1.1 kW), the power of the converters is proportionally decreased/increased. Therefore, the mismatch current between the load and PV are appropriately supported by the converters.

The output voltages of each converter are shown in Fig. 15(c), where the dc link voltage is regulated close to the reference value. The variation of the injected frequency in Fig. 15(d) by the load and PV power variation further demonstrate the performance of the frequency based droop approach. For instance, at t = 2.5 sec, the load current is 7 A, and the PV current is 2.4 A, therefore the converters need to supply 4.6 A. Hence, considering the ratings of the converters, corresponding currents need to be 3.06 and 1.53 A for the first and second converters respectively, which is shown in Fig. 15(a). Therefore, considering the frequency droop gains equal to 0.15 and 0.3, the frequency drop is calculated as 0.46 Hz (see Fig. 14(d))

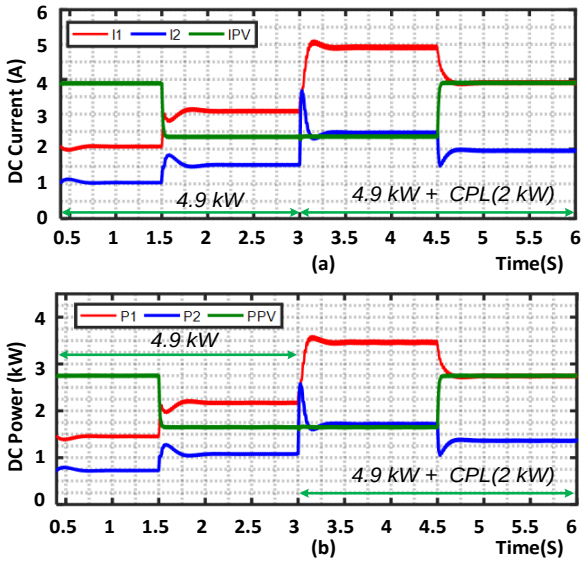

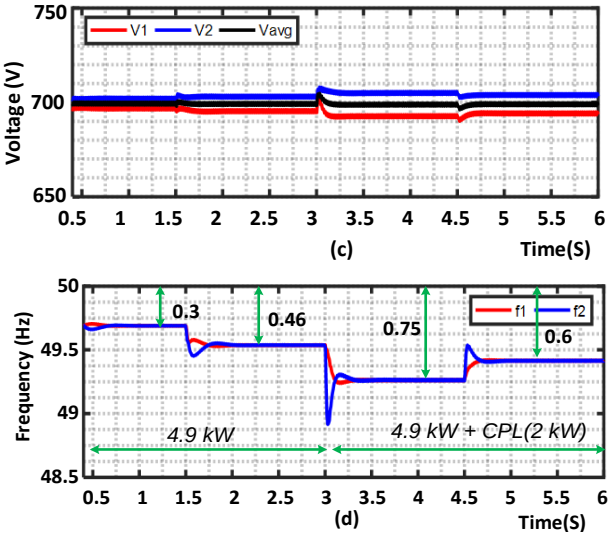

Fig. 14. Simulation results of Case III with PV array; (a) DC current, (b) DC power, (c) mean values of DC voltage of DG1 and DG2 and average of these voltages, (d) Frequency.

VII. Conclusion

This paper has presented a reliable distributed primary and secondary control without any communication network for power management in LVDC microgrids. A merged ac/dc droop controller, as both secondary and primary controller is used for proper power sharing between DGs and maintaining the dc bus voltages within acceptable values. The proposed power sharing controller works without any communication network and therefore, it offers high reliability. The model of the suggested control system is obtained and its stability is analyzed to choose suitable values for the droop gains. The viability of proposed control system is ensured for different line impedances, unequal DG ratings and different dynamic loads including constant impedance, constant current and constant power loads. Moreover, the viability of the proposed control approach is demonstrated in the presence of PV array as a constant power generation unit. The proposed approach is verified by simulations based on MATLAB/Simulink.

Appendix: Inner Control Loops

In this paper, a boost topology is considered for the DC/DC converter to verify the proposed control approach. The electric circuit and the inner voltage and current controllers are shown in Fig. 15. Mathematical representation of the small signal model of the converter with the voltage and current controllers is shown in Fig. 15 [48], [49].

$G_v(s)$ and $G_i(s)$ are the voltage and current PI controllers which can be defined as:

$$G_v(s) = k_{pv} + k_{iv}/s \quad , \qquad G_i(s) = k_{pi} + k_{ii}/s \tag{37}$$

Where s is Laplace operator, k_{pv} and k_{iv} are the proportional and integral gains of the voltage controller and k_{pi} and k_{ii} are the proportional and integral gains of the current controller.

As it can be in Fig. 15, $G_{vd}(s)$ is a small signal open loop

transfer function from the control (i.e, *d*) to the output voltage, and $G_{id}(s)$ is the small signal open loop transfer function from the control to the inductor current. The definition of these transfer functions considering ideal inductor and capacitor are as follows [48]:

$$G_{vd}(s) = \frac{V_o}{(1-D)} \frac{(R(1-D)^2 - L_{dc}s)}{R(1-D)^2 + L_{dc}s + RL_{dc}C_{dc}s^2} \quad (38)$$

$$G_{id}(s) = \frac{2V_o(1+0.5RC_{dc}s)}{R(1-D)^2 + L_{dc}s + RL_{dc}C_{dc}s^2} \quad (39)$$

where C_{dc} and L_{dc} are the boost converter capacitor and inductor, R is the load resistance, Vo is the output voltage and D is the duty cycle.

The closed loop transfer function of the current loop, $G_{cli}(s)$ and the closed loop transfer function of the voltage loop, $G_{clv}(s)$ can be calculated as follows:

$$G_{cli}(s) = \frac{G_i(s)G_{id}(s)}{1+G_i(s)G_{id}(s)} \quad (40)$$

$$G_{clv}(s) = \frac{G_v(s)G_i(s)G_{vd}(s)}{1+G_i(s)G_{id}(s)+G_v(s)G_i(s)G_{vd}(s)} \quad (41)$$

TABLE II

Parameters of DC/DC converters and inner controllers

Definition	Symbol	Value
Input Voltage	V_i *(V)*	540
Output Voltage	V_o *(V)*	700
DC Capacitor	C_{dc} *(μF)*	500
DC Inductor	L_{dc} *(mH)*	2
Switching Frequency	f_{sw} *(kHz)*	20
Current Controller	$k_{pi}+k_{ii}/s$	0.05+1/s
Voltage Controller	$k_{pv}+k_{iv}/s$	1.5+20/s

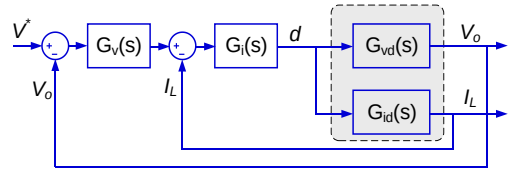

Fig. 15. Block diagram of the inner control loops of boost converter.

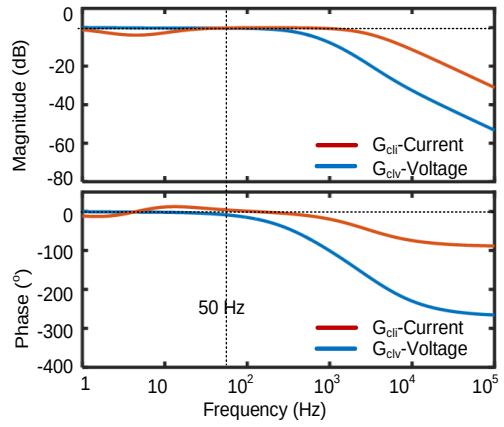

Fig. 16. Closed loop transfer function of inner voltage loop (G_{clv}) and current loop (G_{cli}).

Considering the parameters for the boost converter and controllers like the ones given in Table II, the closed loop transfer functions of the inner voltage and current loops can be obtained. The bode diagram of the closed loop voltage and current transfer functions are illustrated in Fig. 16. As it can be seen in Fig. 16, the voltage controller can effectively track the 50 Hz ac signal which is added to the DC voltage reference. The injected frequency is restricted by the band width frequency of the voltage controller. Therefore, the maximum frequency should be selected lower than the band width frequency of the inner voltage loop.

REFERENCES

[1] B. Kroposki, R. Lasseter, T. Ise, S. Morozumi, S. Papathanassiou, and N. Hatziargyriou, "Making Microgrids Work," *IEEE Power Energy Mag.*, vol. 6, no. 3, pp. 40–53, 2008.

[2] S. Morozumi, "Micro-Grid Demonstration Projects in Japan," *Fourth Power Convers. Conf. PCC-NAGOYA 2007 - Conf. Proc.*, pp. 635–642, 2007.

[3] D. Salomonsson, S. Member, L. Söder, and A. Sannino, "An Adaptive Control System for a DC Microgrid for Data Centers," *IEEE Trans. Ind. Appl.*, vol. 44, no. 6, pp. 1910–1917, 2008.

[4] H. Kakigano, Y. Miura, and T. Ise, "Low-Voltage Bipolar-Type DC Microgrid for Super High Quality Distribution," *IEEE Trans. Power Electron.*, vol. 25, no. 12, pp. 3066–3075, 2010.

[5] Y.-K. Chen, Y.-C. Wu, C.-C. Song, and Y.-S. Chen, "Design and Implementation of Energy Management System With Fuzzy Control for DC Microgrid Systems," *IEEE Trans. Power Electron.*, vol. 28, no. 4, pp. 1563–1570, Apr. 2013.

[6] E. Alliance, "380 Vdc Architectures for the Modern Data Center," 2013. [Online]. Available: http://www.emergealliance.org/. [Accessed: 01-Jan-2016].

[7] S. P. Barave and B. H. Chowdhury, "Hybrid AC/DC Power Distribution Solution for Future Space Applications," *2007 IEEE Power Eng. Soc. Gen. Meet.*, vol. 65401, 2007.

[8] J. Robinson, D. Jovcic, and G. Joós, "Analysis and Design of an Offshore Wind Farm Using a MV DC Grid," *IEEE Trans. Power Deliv.*, vol. 25, no. 4, pp. 2164–2173, 2010.

[9] J. G. Ciezki and R. W. Ashton, "Selection and Stability Issues Associated with a Navy Shipboard DC Zonal Electric Distribution System," *IEEE Trans. Power Deliv.*, vol. 15, no. 2, pp. 665–669, 2000.

[10] C. C. Chan, "An Overview of Electric Vehicle Technology," *Proc. IEEE*, vol. 81, no. 9, pp. 1202–1213, 1993.

[11] N. G. Hingorani, "High-Voltage DC Transmission: A Power Electronics Workhorse," *IEEE Spectr.*, vol. 33, no. 4, pp. 63–72, 1996.

[12] D. Manz, R. Walling, N. Miller, B. LaRose, R. D'Aquila, and B. Daryanian, "The Grid of the Future: Ten Trends That Will Shape the Grid Over the Next Decade," *IEEE Power Energy Mag.*, vol. 12, no. 3. pp. 26–36, 2014.

[13] M. E. Baran and N. R. Mahajan, "DC Distribution for Industrial Systems: Opportunities and Challenges," *IEEE Trans. Ind. Appl.*, vol. 39, no. 6, pp. 1596–1601, 2003.

[14] P. C. Loh, Y. K. Chia, D. Li, and F. Blaabjerg, "Autonomous Operation of Distributed Storages in Microgrids," *IET Power Electron.*, vol. 7, no. 1, pp. 23–30, 2014.

[15] J. Rocabert, A. Luna, F. Blaabjerg, P. Rodriguez, and P. Rodríguez, "Control of Power Converters in AC Microgrids," *IEEE Trans. Power Electron.*, vol. 27, no. 11, pp. 4734–4749, 2012.

[16] S. Anand, B. G. Fernandes, and J. M. Guerrero, "Distributed Control to Ensure Proportional Load Sharing and Improve Voltage Regulation in Low-Voltage DC Microgrids," *IEEE Trans. Power Electron.*, vol. 28, no. 4, pp. 1900–1913, 2013.

[17] T. Zhou and B. François, "Energy Management and Power Control of a Hybrid Active Wind Generator for Distributed Power Generation and Grid Integration," *IEEE Trans. Ind. Electron.*, vol. 58, no. 1, pp. 95–104, 2011.

[18] X. Lu, K. Sun, J. M. Guerrero, J. C. Vasquez, and L. Huang, "State-of-Charge Balance Using Adaptive Droop Control for Distributed Energy Storage Systems in DC Microgrid Applications," *IEEE Trans. Ind. Electron.*, vol. 61, no. 6, pp. 2804–2815, 2014.

[19] J. M. Guerrero, L. GarciadeVicuna, J. Matas, M. Castilla, and J. Miret,

"Output Impedance Design of Parallel-Connected UPS Inverters With Wireless Load-Sharing Control," *IEEE Trans. Ind. Electron.*, vol. 52, no. 4, pp. 1126–1135, Aug. 2005.

[20] A. Tuladhar, H. Jin, T. Unger, and K. Mauch, "Control of Parallel Inverters in Distributed AC Power Systems with Consideration of Line Impedance Effect," *IEEE Trans. Ind. Appl.*, vol. 36, no. 1, pp. 131–138, 2000.

[21] M. Marwali, J. Jung, and A. Keyhani, "Control of Distributed Generation Systems-Part II: Load Sharing Control," *IEEE Trans. Power Electron.*, vol. 19, no. 6, pp. 1551 – 1561, 2004.

[22] Y. A. R. I. Mohamed and E. F. El-Saadany, "Adaptive Decentralized Droop Controller to Preserve Power Sharing Stability of Paralleled Inverters in Distributed Generation Microgrids," *IEEE Trans. Power Electron.*, vol. 23, no. 6, pp. 2806–2816, 2008.

[23] K. De Brabandere, "A Voltage and Frequency Droop Control Method for Parallel Inverters," *IEEE Trans. Power Electron.*, vol. 22, no. 4, pp. 1107 – 1115, 2007.

[24] J. Guerrero and J. Vasquez, "Control Strategy for Flexible Microgrid Based on Parallel Line-Interactive UPS Systems," *IEEE Trans. Ind. Electron.*, vol. 56, no. 3, pp. 726 – 736, 2009.

[25] P. Karlsson and J. Svensson, "DC Bus Voltage Control for a Distributed Power System," *IEEE Trans. Power Electron.*, vol. 18, no. 6, pp. 1405–1412, Nov. 2003.

[26] Y. Ito, Y. Zhongqing, and H. Akagi, "DC Microgrid Based Distribution Power Generation System," *4th Int. Power Electron. Motion Control Conf. 2004. IPEMC 2004.*, vol. 3, pp. 1740–1745, 2004.

[27] P. C. Loh, D. Li, Y. K. Chai, and F. Blaabjerg, "Autonomous Operation of Hybrid Microgrid with AC and DC Subgrids," *IEEE Trans. Power Electron.*, vol. 28, no. 5, pp. 2214–2223, 2013.

[28] H. Laaksonen, "Voltage and Frequency Control of Inverter Based Weak LV Network Microgrid," *Proc. IEEE FPS*, pp. 1–6, 2005.

[29] W. Qiu and Z. Liang, "Practical Design Considerations of Current Sharing Control for Parallel VRM Applications," *Proc. IEEE APEC*, pp. 281 – 286, 2005.

[30] A. Khorsandi, M. Ashourloo, and H. Mokhtari, "A Decentralized Control Method for a Low-Voltage DC Microgrid," *IEEE Trans. Energy Convers.*, vol. 29, no. 4, pp. 793–801, 2014.

[31] T. L. Vandoorn, S. Member, and B. Meersman, "A Control Strategy for Islanded Microgrids With DC-Link Voltage Control," *IEEE Trans. Power Deliv.*, vol. 26, no. 2, pp. 703–713, 2011.

[32] J. M. Guerrero, J. C. Vasquez, J. Matas, L. G. De Vicuña, and M. Castilla, "Hierarchical Control of Droop-Controlled AC and DC Microgrids - A General Approach toward Standardization," *IEEE Trans. Ind. Electron.*, vol. 58, no. 1, pp. 158–172, 2011.

[33] T. Dragicevic, J. M. Guerrero, J. C. Vasquez, and D. Skrlec, "Supervisory Control of an Adaptive-Droop Regulated DC Microgrid with Battery Management Capability," *IEEE Trans. Power Electron.*, vol. 29, no. 2, pp. 695–706, 2014.

[34] Q. Shafiee, J. M. Guerrero, and J. C. Vasquez, "Distributed Secondary Control for Islanded Microgrids—A Novel Approach," *IEEE Trans. Power Electron.*, vol. 29, no. 2, pp. 1018–1031, 2014.

[35] X. Lu, J. M. Guerrero, K. Sun, and J. C. Vasquez, "An Improved Droop Control Method for DC Microgrids Based on Low Bandwidth Communication With DC Bus Voltage Restoration and Enhanced Current Sharing Accuracy," *IEEE Trans. Power Electron.*, vol. 29, no. 4, pp. 1800–1812, Apr. 2014.

[36] V. Nasirian, A. Davoudi, and F. L. Lewis, "Distributed Adaptive Droop Control for Dc Microgrids," *IEEE Trans. Energy Convers.*, vol. 29, no. 4, pp. 1147–1152, 2014.

[37] D. Perreault, R. Selders, and J. Kassakian, "Frequency-Based Current-Sharing Techniques for Paralleled Power Converters," *IEEE Trans. Power Electron.*, vol. 13, no. 4, pp. 626 – 634, 1998.

[38] M. Angjelichinoski and C. Stefanovic, "Power Talk: How to Modulate Data over a Dc Micro Grid Bus Using Power Electronics," *arXiv Prepr. arXiv 1504.03016*, 2015.

[39] A. Tuladhar, H. Jin, T. Unger, and K. Mauch, "Parallel Operation of Single Phase Inverter Modules with No Control Interconnections," in *Proc. IEEE APEC*, 1997, vol. 1, pp. 94–100.

[40] A. Tuladhar and H. Jin, "A Novel Control Technique to Operate DC/DC Converters in Parallel with No Control Interconnections," in *Proc. IEEE PESC*, 1998, vol. 1, pp. 892–898.

[41] J. Glover, M. Sarma, and T. Overbye, "*Power Systems Analysis and Design*," 4th ed. Thomson Learning, 2008.

[42] Y. W. Li and C.-N. Kao, "An Accurate Power Control Strategy for Power-Electronics-Interfaced Distributed Generation Units Operating in a Low-Voltage Multibus Microgrid," *IEEE Trans. Power Electron.*, vol. 24, no. 12, pp. 2977–2988, Dec. 2009.

[43] J. He and Y. W. Li, "Analysis, Design, and Implementation of Virtual Impedance for Power Electronics Interfaced Distributed Generation," *IEEE Trans. Ind. Appl.*, vol. 47, no. 6, pp. 2525–2538, 2011.

[44] H. Nikkhajoei and R. Iravani, "Steady-State Model and Power Flow Analysis of Electronically-Coupled Distributed Resource Units," *2007 IEEE Power Eng. Soc. Gen. Meet. PES*, vol. 22, no. 1, pp. 721–728, 2007.

[45] J. M. Guerrero, L. Hang, and J. Uceda, "Control of Distributed Uninterruptible Power Supply Systems," *IEEE Trans. Ind. Electron.*, vol. 55, no. 8, pp. 2845–2859, 2008.

[46] D. Dong, D. Boroyevich, R. Wang, and I. Cvetkovic, "A Two-Stage High Power Density Single-Phase Ac-Dc Bi-Directional PWM Converter for Renewable Energy Systems," in *Proc. IEEE ECCE*, 2010, pp. 3862–3869.

[47] D. Boroyevich, I. Cvetković, D. Dong, R. Burgos, F. Wang, and F. Lee, "Future Electronic Power Distribution Systems - A Contemplative View," *Proc. Int. Conf. Optim. Electr. Electron. Equipment, OPTIM*, pp. 1369–1380, 2010.

[48] D. He and R. Nelms, "Peak Current-Mode Control for a Boost Converter Using an 8-Bit Microcontroller," *IEEE PESC*, 2003.

[49] R. Erickson and D. Maksimovic, "*Fundamentals of Power Electronics*." Springer Science & Business Media, 2007.